Postbuckling Behavior of Laminated Plates Using a Direct Energy-Minimization Technique

Pierre J. Minguet,* John Dugundji,† and Paul Lagace‡
Massachusetts Institute of Technology, Cambridge, Massachusetts

The postbuckling behavior of rectangular, flat, laminated, or sandwich plates is investigated using a model including the different anisotropic material coupling terms, the effect of transverse shear deformation, nonlinear strains, and initial out-of-plane imperfections. The Rayleigh-Ritz method is used to discretize the problem and, instead of solving a set of partial-differential equations, a direct energy-minimization technique is used to solve the problem numerically. The solution procedure used is described in detail in the first part of this paper, and the results obtained for three example problems are presented in the second part. These results correlate well with corresponding experimental data that are also presented.

I. Introduction

WITH the increased consideration of composite materials for use in primary aircraft structures, old issues such as plate buckling must be given renewed attention because of the unique problems introduced by the anisotropy of composites. Furthermore, since composite materials usually do not exhibit large yielding deformations prior to failure and therefore do not allow stresses to be redistributed in the postbuckling region, simple design procedures developed for metallic panels (such as the equivalent-width concept) can no longer be used. Thus, a more detailed analysis in the postbuckling region is needed to predict fully the behavior of composite plates.

A recent report by Leissa[1] contains over 400 references relative to laminated and sandwich plate and shell buckling. Most of the literature on the buckling of sandwich panels can be separated into two areas. The first is the formulation of accurate plate models that take into account the shear deformation of the plate cross section: from the original Reissner[2]–Mindlin[3] work that assumes a linear variation of stresses and strains through the thickness to more recent, higher-order theories, for example, a recent paper by Reddy.[4] These, however, can quickly lead to some very complicated algebra and also get computationally expensive since more variables are needed to describe the displacement fields. The second aspect is the evaluation of the critical buckling loads for various types of instabilities: from the overall buckling problem, as in Ref. 5, to its combination and interaction with face wrinkling for sandwich panels as in Ref. 6. Also, with the introduction of composite materials, new problems for the analysis arise from the different coupling terms that can result from the possibility of having completely anisotropic panels, which makes the determination of closed-form solutions unlikely or cumbersome. Although much work has already been done in this area, most references are still concerned only with obtaining critical loads, that is, solving the linear eigenvalue problem. Few of them, as for instance Ref. 7 for laminated plates, are concerned with the actual load response of panels, which requires solving the nonlinear, large deflection plate equations.

The objective of this paper is twofold: first, to present a simple and efficient solution technique for structural problems involving geometric nonlinearities, and second, to use this procedure to calculate and illustrate by some examples the postbuckling behavior of laminated plates. As will be shown, the computer program that was developed allows one to get a rapid idea of the behavior of a flat, rectangular panel under load, which could make it useful, for example, in a preliminary design stage where an efficient analysis is needed to evaluate many different laminate designs. A more complete description of the analysis can be found in Ref. 8.

II. Formulation

Since composite materials are more sensitive to transverse shear deformation because of their low shear modulus and in order to analyze sandwich plates, a Reissner-Mindlin-type plate model will be used, i.e., normal planar sections will remain planar during deformation but not normal to the midplane. Thus, displacements in the plate can be written as

$$u_p(x, y, z) = u(x, y) + z\phi(x, y)$$
$$v_p(x, y, z) = v(x, y) + z\theta(x, y)$$
$$w_p(x, y, z) = w(x, y) \tag{1}$$

where u_p, v_p, w_p are displacements anywhere in the plate; u, v, w displacements of the midplane; and ϕ, θ rotations.

Since a potential energy formulation will be used, the plate behavior will be described in terms of the three midplane displacements u, v, w and the two rotations ϕ, θ, instead of using a stress function to describe the in-plane behavior. For the postbuckling behavior, nonlinear strain-displacement relations must be used

$$\varepsilon_{ij} = \frac{1}{2}\left(\frac{\partial u_i}{\partial x_j} + \frac{\partial u_j}{\partial x_i} + \frac{\partial u_k}{\partial x_i}\frac{\partial u_k}{\partial x_j}\right) \tag{2}$$

If the in-plane displacements remain small and transverse displacement remains moderate, a look at the relative orders of magnitude of the different terms allows one to neglect the in-plane rotations and simplify these relations to the usual von Karman equations for large deflections. Combining these

Received May 7, 1988; revision received Jan. 10, 1989.

*Research Assistant, Technology Laboratory for Advanced Composites, Department of Aeronautics and Astronautics.

†Professor, Department of Aeronautics and Astronautics. Member AIAA.

‡Associate Professor, Department of Aeronautics and Astronautics. Member AIAA.

equations with Eqs. (1) gives the final form of the strain-displacement relations

$$\varepsilon_{11} = u_{,x} + \tfrac{1}{2}(w_{,x})^2 + w_{0,x}w_{,x} + z\phi_{,x}$$
$$\varepsilon_{22} = v_{,y} + \tfrac{1}{2}(w_{,y})^2 + w_{0,y}w_{,y} + z\theta_{,y}$$
$$\gamma_{12} = u_{,y} + v_{,x} + w_{,x}w_{,y} + w_{0,x}w_{,y} + w_{0,y}w_{,x} + z(\phi_{,y} + \theta_{,x})$$
$$\gamma_{13} = \phi + w_{,x}$$
$$\gamma_{23} = \theta + w_{,y} \tag{3}$$

where w_0 is the initial transverse displacement and $\gamma_{ij} = 2\varepsilon_{ij}$ are the engineering shear strains.

The material stress-strain behavior is assumed to be linear. If $\boldsymbol{N}$ and $\boldsymbol{M}$ are defined as the usual force and moment resultant vectors, the plate material behavior can be described with the same relations as in classical laminated plate theory

$$\boldsymbol{N} = A\boldsymbol{\varepsilon}^0 + B\boldsymbol{K}$$
$$\boldsymbol{M} = B\boldsymbol{\varepsilon}^0 + D\boldsymbol{K}$$

where

$$(A_{ij}, B_{ij}, D_{ij}) = \int_{-h/2}^{+h/2} C_{ij}(1, z, z^2)\,\mathrm{d}z \tag{4}$$

Midplane strains

$$\boldsymbol{\varepsilon}^0 = (\varepsilon^0_{11}, \varepsilon^0_{22}, \gamma^0_{12})^T$$

Curvatures

$$\boldsymbol{K} = (\phi_{,x}, \theta_{,y}, \phi_{,y} + \theta_{,x})^T$$

No limitations need be done on these terms and all coupling terms are here taken into account. Similarly, if $\boldsymbol{Q}$ is defined as the transverse shear forces' resultant, the last two stress-strain relations should be written as follows to be consistent with the assumed displacement fields:

$$\boldsymbol{Q} = G\boldsymbol{\gamma} \tag{5}$$

However, it is well known that this would overestimate the stiffness. The classical way, as shown by Reissner, to correct this for isotropic materials is to use a shear correction factor of 5/6. For laminated plates, two shear correction factors k_1 and k_2 can be determined using, for example, the procedure described by Whitney in Ref. 9. The shear stress-strain relations are then simply rewritten as

$$\begin{bmatrix} Q_y \\ Q_x \end{bmatrix} = \begin{bmatrix} G_{44} & G_{45} \\ G_{45} & G_{55} \end{bmatrix} \begin{bmatrix} \gamma_4 \\ \gamma_5 \end{bmatrix} = \begin{bmatrix} k_1^2 A_{44} & k_1 k_2 A_{45} \\ k_1 k_2 A_{45} & k_2^2 A_{55} \end{bmatrix} \begin{bmatrix} w_{,y} + \theta \\ w_{,x} + \phi \end{bmatrix} \tag{6}$$

The principle of the minimum of the potential energy Π_p will be used here to solve the problem

$$\min_u \Pi_p = \min_u \left(\frac{1}{2} \int_V C_{ij}\varepsilon_i\varepsilon_j\,\mathrm{d}V - \int_S f_i u_i\,\mathrm{d}S \right) \tag{7}$$

If we introduce all of the assumptions just stated, the plate strain energy can be expressed as a function of the five unknowns u, v, w, ϕ, θ after integration through the thickness

$$U = \frac{1}{2} \iint (\boldsymbol{\varepsilon}^{0T}[A]\boldsymbol{\varepsilon}^0 + 2\boldsymbol{\varepsilon}^{0T}[B]\boldsymbol{\kappa} + \boldsymbol{\kappa}^T[D]\boldsymbol{\kappa} + \boldsymbol{\gamma}^T[G]\boldsymbol{\gamma})\,\mathrm{d}x\,\mathrm{d}y \tag{8}$$

If the midplane strain $\boldsymbol{\varepsilon}^0$ is separated into its linear and nonlinear parts, $\boldsymbol{\varepsilon}_1$ and $\boldsymbol{\varepsilon}_{n1}$, the strain energy can be broken down into different components U_i, and each can be identified as having a specific meaning as follows:

$$U_1 = \frac{1}{2} \iint \boldsymbol{\varepsilon}_1^T[A]\boldsymbol{\varepsilon}_1\,\mathrm{d}x\,\mathrm{d}y \tag{9}$$

U_1 is a quadratic term representing the in-plane stretching of the plate, that is, the membrane behavior.

$$U_2 = \frac{1}{2} \iint 2\boldsymbol{\varepsilon}_1^T[A]\boldsymbol{\varepsilon}_{n1}\,\mathrm{d}x\,\mathrm{d}y \tag{10}$$

U_2 is a geometric coupling between in- and out-of-plane deformations. This term "causes" buckling and is the one that is included to solve the linear eigenvalue problem.

$$U_3 = \frac{1}{2} \iint \boldsymbol{\varepsilon}_{n1}^T[A]\boldsymbol{\varepsilon}_{n1}\,\mathrm{d}x\,\mathrm{d}y \tag{11}$$

U_3 is a fourth-order term in w that represents the postbuckling stiffness of the plate.

$$U_4 = \frac{1}{2} \iint 2\boldsymbol{\varepsilon}_1^T[B]\boldsymbol{\kappa}\,\mathrm{d}x\,\mathrm{d}y \tag{12}$$

U_4 is a quadratic term representing the material coupling between in- and out-of-plane deformations that occurs in unsymmetric plates.

$$U_5 = \frac{1}{2} \iint 2\boldsymbol{\varepsilon}_{n1}^T[B]\boldsymbol{\kappa}\,\mathrm{d}x\,\mathrm{d}y \tag{13}$$

U_5 is a complement of the previous one U_4 for the nonlinear part of the in-plane strains.

$$U_6 = \frac{1}{2} \iint \boldsymbol{\kappa}^T[D]\boldsymbol{\kappa}\,\mathrm{d}x\,\mathrm{d}y \tag{14}$$

U_6 is a quadratic term representing the bending stiffness of the plate.

$$U_7 = \frac{1}{2} \iint \boldsymbol{\gamma}^T[G]\boldsymbol{\gamma}\,\mathrm{d}x\,\mathrm{d}y \tag{15}$$

U_7 is a quadratic term representing the plate transverse shear stiffness. Notice this is the only term coupling w with ϕ and θ, and also the only one containing terms that are functions of w alone. This will mean that if G gets smaller and smaller, the plate will lose all transverse stiffness even if D is not zero.

Finally, there is also W, the work term contribution to the potential energy Π_p, expressed as

$$W = \iint pw\,\mathrm{d}x\,\mathrm{d}y + \int \bar{\boldsymbol{N}}^T \cdot \boldsymbol{u}\,\mathrm{d}s \tag{16}$$

with p, distributed transverse pressure, and $\bar{\boldsymbol{N}}^T$ applied forces at the boundary.

In addition to these terms, there are several other contributions to the potential energy from the initial imperfections w_0 that are not indicated here for clarity. These terms are very similar to those just shown and can be obtained by substituting w_0 for w at appropriate places [see Eqs. (3)].

III. Boundary Conditions

No discussion for a solid mechanics problem would be complete without a word about boundary conditions. Since the potential energy approach is used here, mention will be made only of the geometric ones that need to be satisfied. They can be separated into two categories.

1) Out-of-plane, concerning w, θ_n, and θ_s (rotations normal and tangent to the boundary): free, no restrictions on w,

θ_n, θ_s; simply supported, $w = 0$, no restrictions on θ_n, θ_s; clamped, $w = 0$, $\theta_n = 0$, $w_{,n} = 0$.

2) In-plane, concerning u_n and u_s. These are also important, although not as obvious as the out-of-plane conditions, and different choices can lead to completely different behavior in the postbuckling range: straight edge, u_n must be constant along that edge (but not necessarily zero); stress-free edge, u_n and u_s must be free to take arbitrary values; uniformly loaded edge, same condition, u_n and u_s arbitrary.

To illustrate these in-plane conditions, consider the following three cases:

1) All edges are constrained to remain straight (for example, if the plate was surrounded by strong stiffeners). This is the stiffest case since tensile membrane stresses develop at the middle of the lateral (unloaded) edges and tend to pull the plate back in. (Notice, no overall load is applied on the lateral edges.)

2) The lateral edges are now no longer constrained to be straight, but are free to deform, and since the foregoing stresses have been released, stiffness decreases significantly. The loaded edges are kept straight and the applied load tends to redistribute outward toward their ends.

3) The lateral edges are still free to deform, but now the loaded ones are also no longer constrained to be straight so that the applied load tends to remain uniformly distributed. This causes higher stresses at the middle of these edges than in the previous case, and since the plate is "softer" there, this causes larger out-of-plane deflections.

Notice that these three different conditions have no effect on the buckling load but only the postbuckling stiffness. These are significant effects and should not be overlooked when comparing results from different analyses or experiments.

IV. Minimization Technique

At this point, the usual way of proceeding would be to take the variation of the potential energy over the five unknown fields to obtain a set of five nonlinear, partial-differential equations that could be solved using, for example, Galerkin's method. Here, a different approach is taken. First, a discrete expression of the potential energy is obtained. Since only rectangular plates are being considered here, the Rayleigh-Ritz method is used for this purpose and several series of modes are assumed for each unknown. The resulting expression, once all integrations have been performed, can be represented as a fourth-order polynomial in the unknown modal amplitude q_i

$$F(q_i) = \sum f_i q_i + \sum K_{ij} q_i q_j + \sum K_{ijk} q_i q_j q_k + \sum K_{ijkl} q_i q_j q_k q_l \quad (17)$$

Then, one minimizes directly this function using a "minimum-seeking" algorithm in order to find the equilibrium points. All of these algorithms usually proceed in an iterative way, each iteration being divided into three steps.

1) At iteration n from a current point $\boldsymbol{q}_n$, find a vector $\boldsymbol{s}_n$, called "descent direction" so that the function $F(\boldsymbol{q})$ is decreasing along it, that is,

$$\nabla F_n \cdot \boldsymbol{s}_n < 0$$

where $\nabla F_n = \{\partial F/\partial q_i\}_n$ is the gradient of F at $\boldsymbol{q}_n$.

2) Along that line, find the absolute minimum of $F(\boldsymbol{q})$, that is, solve the equation

$$\frac{\mathrm{d}}{\mathrm{d}\alpha}[F(\boldsymbol{q}_n + \alpha \boldsymbol{s}_n)] = 0 \quad (18)$$

This operation is often called "line search" and its solution α_n represents the optimum step length that can be made in that direction, that is, the one that will give the largest decrease in value for $F(\boldsymbol{q})$.

3) Increment the unknowns to that new point

$$\boldsymbol{q}_{n+1} = \boldsymbol{q}_n + \alpha \boldsymbol{s}_n$$

and start over again until convergence is reached, that is, if the magnitude of the gradient vector ∇F_n at that point is below a certain level.

Most algorithms will differ on the way they find the descent direction in step 1. Two (among many) of the most popular methods for this are the conjugated gradient method and the Newton-Raphson method. The first method requires only the evaluation of the gradient ∇F_n at each iteration that makes it very affordable computationally. However, since it is a first-order method, its convergence can be sometimes slow. For the second method, the descent direction is defined as

$$\boldsymbol{s}_n = -H_n^{-1} \cdot \nabla F_n \quad (19)$$

where $H_n = [\partial^2 F/\partial q_i \partial q_j]_n$ is the Hessian of F at $\boldsymbol{q}_n$.

This method usually converges very fast, but since it requires the evaluation and inversion of the Hessian matrix at every iteration, it is more costly and its use is restricted generally to problems with a relatively small number of unknowns. Since this was the case here, this second method was used.

Once a suitable descent direction $\boldsymbol{s}_n$ has been determined at a point $\boldsymbol{q}_n$, it is possible to improve the convergence of the algorithm in step 2 by trying to find the absolute minimum of the function $F(\boldsymbol{q})$ along the line defined by $\boldsymbol{s}_n$. This can sometimes be a very expensive operation if $F(\boldsymbol{q})$ is not known explicitly, but in the present case, a great simplification arises from the fact that $F(\boldsymbol{q})$ is a fourth-order polynomial so that

$$F(\boldsymbol{q}_n + \alpha \boldsymbol{s}_n) = a_4\alpha^4 + a_3\alpha^3 + a_2\alpha^2 + a_1\alpha + F(\boldsymbol{q}_n) \quad (20)$$

where α is the step length.

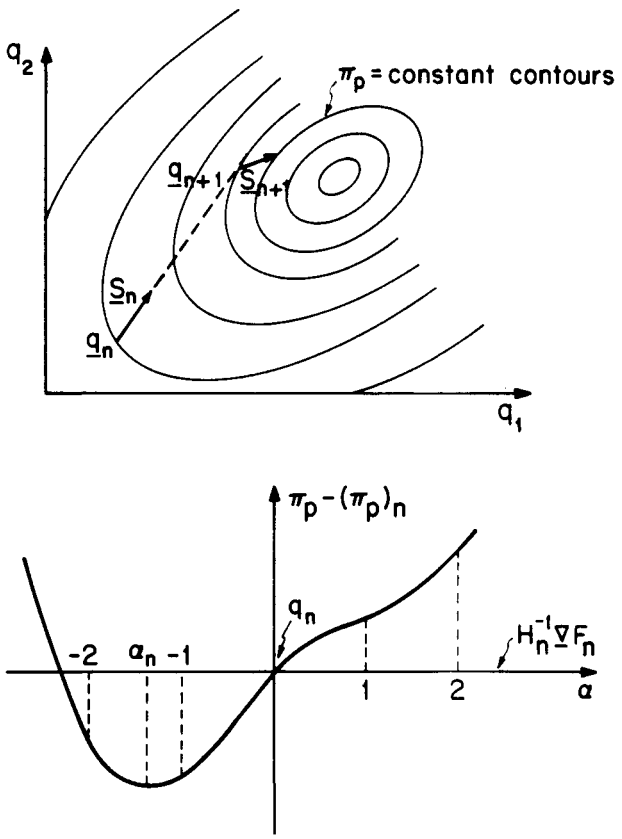

Fig. 1 Illustration of energy-minimization procedure (top) for a two-variables problem and of the line-search technique (bottom).

Finding the optimal step length α_n then reduces to finding the roots of a third-order polynomial that is the derivative of Eq. (20). This gives the stationary points of the polynomial, Eq. (20). A simple way of evaluating the coefficients a_i of this polynomial is to evaluate $F(\boldsymbol{q}_n + \alpha \boldsymbol{s}_n)$ for different values of α, namely, -2, -1, 0, 1, 2, and then to find the polynomial passing through these points (as illustrated in Fig. 1).

This "line-search" technique for optimal α_n was used here. If the line-search technique of step 2 is omitted by simply setting $\alpha = 1$, one obtains the conventional Newton-Raphson iteration, but the convergence is then slower.

The direct minimization technique used here offers a few advantages over the other classical methods. First, it is a direct application of the minimum principles and its formulation is easier to interpret physically. It is very simple to use since no long algebraic developments are needed: For a given problem, it is only necessary to write down the corresponding expression for the potential energy. It is also very easy to extend this procedure to other types of models: The original model used to develop this method was a Kirchhoff plate model to analyze thin plates. The extension to the Reissner-Mindlin model was done by adding the terms corresponding to the shear deformation and reorganizing some other terms. Similarly, the extension to cylindrical panels could be done by including in the potential energy the terms containing the radius of curvature. The coding of this method into a computer program is relatively straightforward, although some "bookkeeping" is required to store all the matrices involved: Once a set of mode shapes has been chosen, the different matrices corresponding to the seven terms in the strain energy are calculated by numerical integration. For the minimization algorithm, it is only necessary to be able to calculate, at a given point $\boldsymbol{q}_n$, the value of the function $\Pi(\boldsymbol{q}_n)$, its gradient and its second derivatives. Another advantage of this formulation is that no incremental loading is needed: The solution for a given loading can be obtained directly, which often can save much computation time.

An important issue also with nonlinear problems is the case where multiple solutions, that is, multiple equilibrium points or local minima, can exist for a given load. For example, for the postbuckling problem, transitions from one type of solution to another can occur at some load levels. Since a minimization algorithm cannot usually detect the absolute minimum of a function, something must be done to capture this kind of behavior. Two observations on this problem have been noted from experience. First, the minimization algorithms tend to converge toward the local minimum that is closest to the starting point. Some solution methods based on that observation use a certain number of randomly chosen starting points in the solution space and then compare the local minimum points that were attained from these starting points. Second, for the plate buckling problem, transitions between solution types always occur between deformed shapes close to the buckling eigenmodes of the plate. Therefore, the following procedure was adopted:

1) For the given load, the corresponding linear solution was formed. Usually, for a symmetrical panel, this would correspond to a uniform state of strain.

2) By using the first eigenmode as a descent direction, a line-search operation was done. If a new point resulting in a decrease in potential energy was obtained, the minimization procedure was started from that point until equilibrium was reached. That solution and its energy level were then stored. The whole process was repeated using the second and following eigenvectors. For plates well into the postbuckling range, three trial vectors seemed to be a practical maximum, whereas for sandwich or thick plates, one was usually used in the prebuckling range and two trial vectors were used above the buckling load. Physically, the process can be viewed as loading the plate while holding it flat and then giving it a small perturbation in the shape of the eigenmodes to see if any stable position can be reached.

3) Once all the trial vectors have been used, the energy level of the different solutions was compared and the lowest value obtained was retained as the absolute minimum.

V. Discretization and Displacement Modes

All the information necessary on how to calculate the potential energy Π_p as a function of the five variables u, v, w, ϕ, and θ, and to solve the problem in discrete form has been presented. The last question is to decide which shape functions should be used to represent the displacements: This always involves a part of trial and error, and the choice that was finally adopted is next described.

In-Plane Displacements u, v

These displacements contain two different parts: First, three modes (one for u, two for v) are needed to represent a uniform extensional strain in the x and y directions and a uniform shear strain. The second part is a series of cosine and sine functions: Not all indices i,j are used since experience showed some modes were always negligible, and the actual choice used in the examples is indicated in Table 1.

$$u = u_1 \xi + \sum_i \sum_j u_{ij} \sin(i\pi\xi) \cos(j\pi\eta)$$

$$v = v_1 \eta + v_2 \xi + \sum_i \sum_j v_{ij} \cos(i\pi\xi) \sin(j\pi\eta) \qquad (21)$$

with

$$\xi = \frac{x}{a}, \qquad \eta = \frac{y}{b}$$

As can be seen, those functions are such that all edges of the plate remain straight. For the case where the unloaded (e.g.,

Table 1 In-plane mode shapes

$u = u_{kl} \sin(k\pi\xi) \cos(l\pi\eta)$

k \ l	0	1	2	3	4	5	6	7
1		X		X		X		X
2	X		X		X		X	
3		X		X		X		X
4	X		X		X		X	

$v = v_{kl} \cos(k\pi\xi) \sin(l\pi\eta)$

k \ l	1	2	3	4
0		X		X
1	X		X	
2		X		X
3	X		X	
4		X		X
5	X		X	
6		X		X
7	X		X	

X = Mode used.

$y = 0, b$) edges are free to pull in or out (which was the case in the experiments), the following modes were added:

$$v_f = \sum_i v_{fi} \cos(i\pi\xi)\left(\eta - \frac{1}{2}\right)^3, \qquad i = 1, 4 \tag{22}$$

However, these modes alone cause unwanted shear strains (and stresses) along those same edges and violate the stress-free condition since

$$\frac{\partial v}{\partial x} f = \sum_i v_{fi} \frac{i\pi}{a} \sin(i\pi\xi)\left(\eta - \frac{1}{2}\right)^3 \neq 0 \quad \text{at} \quad \eta = 0, 1 \tag{23}$$

To avoid this, four modes are added to u with a similar form so that it will be possible to minimize these shear strains

$$u_f = \sum_i u_{fi} \sin(i\pi\xi)\left(\eta - \frac{1}{2}\right)^2 \tag{24}$$

Notice that this choice still keeps the loaded edges ($x = 0, a$) straight.

Out-of-Plane Displacements w, ϕ, θ

First, consider the case where the loaded edges are clamped and the others simply supported (the model used to represent the actual experiments is shown later). A separable solution was assumed here, using "beam functions" in the x direction (to satisfy $\partial w/\partial x = 0$ at $x = 0$, a) and sines in the other direction

$$w_{cs} = \sum_i \sum_j w_{ij} F_i(\xi) \sin(j\pi\eta) \tag{25}$$

where

$$F_i(\xi) = \cosh(\alpha_i\xi) - \cos(\alpha_i\xi) - \gamma_i[\sinh(\alpha_i\xi) - \sin(\alpha_i\xi)]$$

and the constants α_i and γ_i are given in Table 2. Alternatively, the beam modes can be represented using the simpler and numerically more accurate expression of Ref. 10.

Normally, the choice of modes for ϕ and θ could be arbitrary (with the condition that $\phi = 0$ at $x = 0$, a), but when the thickness of the plate decreases, one must recover the Kirchhoff condition and the shear strains must vanish. Thus, one should have

$$\varepsilon_5 = \phi + w_{,x} \to 0$$

$$\varepsilon_4 = \theta + w_{,y} \to 0$$

For this to be true everywhere, one should choose

$$\phi_{cs} = \sum_i \sum_j \phi_{ij} \frac{1}{a} F_i'(\xi) \sin(j\pi\eta)$$

$$\theta_{cs} = \sum_i \sum_i \theta_{ij} F_i(\xi) \frac{j\pi}{b} \cos(j\pi\eta) \tag{26}$$

Table 2 Beam functions coefficients, $F(x) = \cosh(\alpha_i x) - \cos(\alpha_i x) - \gamma_i[\sinh(\alpha_i x) - \sin(\alpha_i x)]$

i	Alpha	Gamma
1	4.7300407448627	0.98250221457624
2	7.8532046240958	1.00077731190727
3	10.995607838002	0.99996645012541
4	14.137165491257	1.00000144989766
5	17.278759657400	0.99999993734438

where

$$F_i'(\xi) = \frac{\partial F_i}{\partial \xi}$$

Otherwise, stiffness would get overestimated when the plate thickness decreases (shear locking).

Other types of boundary conditions can be handled similarly using the same basic functions (see Appendix B). Once a set of modes has been chosen, they can be placed into the strain-energy expressions [Eqs. (9–16)] and integrated over the plate area to obtain the final discrete expression of the potential energy. The integrations needed to obtain these matrices were performed using Simpson's parabolic rule.

VI. Examples

A computer program has been written to execute all the operations. Its structure is fairly simple and performs all the steps explained so far.[11] The code is over 2000 Fortran statements long: Its structure is very modular and could be easily modified to include, for instance, other types of boundary conditions or other energy terms to represent different types of panels. In its current version, the program can analyze any rectangular plate made of any stacking sequence. The user has to supply the necessary material properties and geometric sizes, and choose the boundary conditions and number of modes to be used for the different variables. All the stiffness matrices are then generated. Great care was taken in doing this to avoid calculating the same terms several times since those matrices contain numerous symmetrical combinations of indices, therefore saving some valuable time. Once this is done, a load case and some initial imperfection can be applied, and the corresponding solution found.

Table 3 Material properties

AS4/3501-6 graphite-epoxy
E_L: 139.3 GPa E_T: 11.1 GPa G_{LT}: 6.0 GPa ν_{LT}: 0.3 Ply thickness: 0.134 mm
Nomex honeycomb
G_{xz}: 60.0 MPa G_{yz}: 30.0 MPa

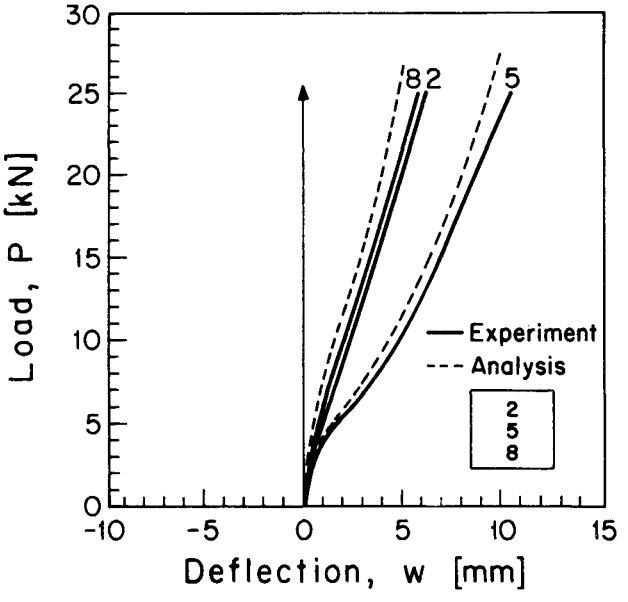

Fig. 2 Load deflection behavior of $[0_2/45_2/0]_s$ plate.

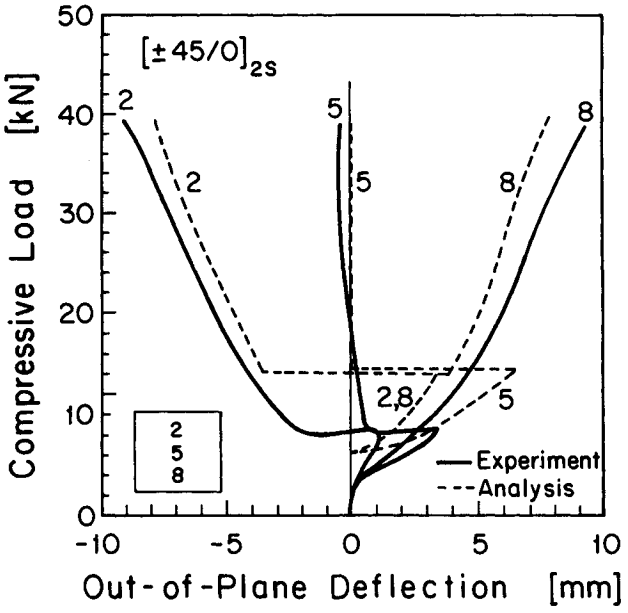

Fig. 3 Load deflection behavior of $[\pm 45/0]_{2s}$ plate.

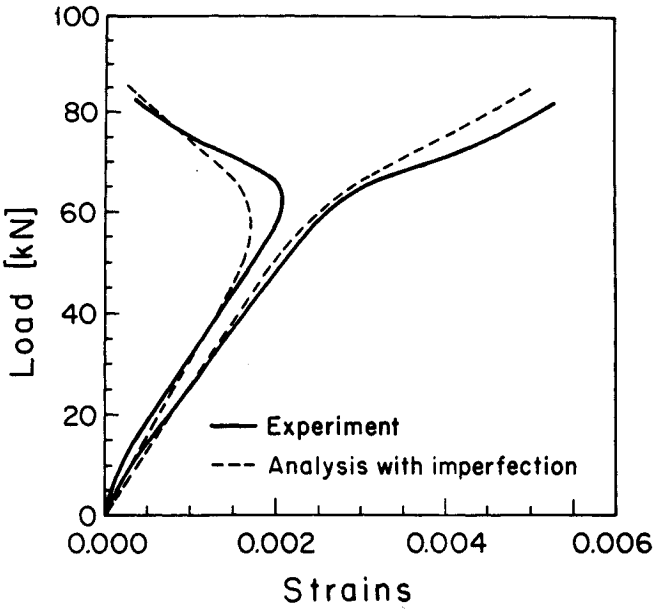

Fig. 5 Load strain behavior of sandwich plate.

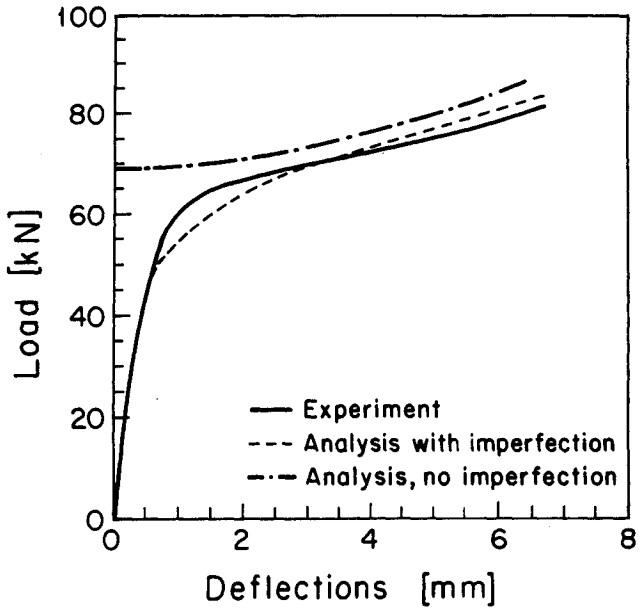

Fig. 4 Load deflection behavior of sandwich plate.

Three examples of the use of this program are shown here. They were chosen partly because of the availability of experimental data that made some assessment of the accuracy of the method possible. The first two concern thin laminated plates in which transverse shear deformation is relatively unimportant, and the third one is a sandwich plate. Sixty-two displacement modes were used for the first case, 85 for the second, and 62 for the third case. All three plates had a test section of 255 × 255 mm and the nominal ply properties used in the analysis for Hercules AS4/3501-6 graphite-epoxy are indicated in Table 3. The computation time involved, on a DEC VAX 11/780, was of the order of 10 CPU min for the second example and approximately 5 min for the first and third.

The layup of the first laminate is $[0_2/45_2/0]_s$. A plot of the load vs transverse deflection behavior is shown in Fig. 2 for the present analysis and the experimental data of Ref. 12. The boundary conditions are considered to be clamped on all four sides. Because this is a fairly thin laminate, its buckling load is fairly low and there is a long postbuckling behavior, which illustrates well the importance of being able to design panels in the postbuckling region to take advantage of that load-carrying capability. From Fig. 2, one can see that the present analysis agrees well with the experimental data but is a little too stiff.

For the second example, a $[\pm 45/0]_{2s}$ layup was analyzed and compared to the experimental data of Ref. 13, as shown in Fig. 3. For this plate, the loaded edges are clamped and the sides simply supported. The interesting point here is that these square panels buckled first in a usual first mode and then, at a higher load, exhibited a transition into a second buckling mode. In order to capture this behavior, a larger number of displacement modes were used, with up to four harmonics in the loading direction for w. With the foregoing technique, solutions corresponding to the first and second buckling mode are obtained: Between a load of approximately 7 and 14 kN, the first mode solution leads to the lowest potential energy, whereas above 14 kN, the second mode has a lower potential energy and is therefore chosen. This example illustrates well the versatility of the present method for problems in which multiple equilibrium points are present.

The last example shown is a sandwich panel with two $[\pm 45/0]_s$ faces and a 3.2 mm thick Nomex honeycomb core, with the loaded edges clamped and the sides simply supported, as in Ref. 14. The load vs center deflection behavior is shown in Fig. 4, as well as the strains measured at the center of the panel in Fig. 5. Because this panel is much stiffer than the previous plates, its buckling load is higher but the postbuckling behavior is more limited. Also, the presence of initial eccentricities has a much more important effect. In the analysis shown, the magnitude of the initial out-of-plane displacements was chosen so that the analysis matches the initial linear portion of the load deflection curve.

VII. Conclusions

An efficient technique to solve the large deflection of plates problem has been presented. The equations used are similar to von Kármán's and Mindlin's plate equations and are discretized with the Rayleigh-Ritz method, and solved with a minimization algorithm. Some of the advantages of this formulation are that it is easy to implement and expand, no incremental loading is necessary, and it is able to handle cases in which multiple equilibrium points are present. The method is also relatively fast, which could make it a good tool in a preliminary design stage when many candidate laminates must

be evaluated and compared. From the examples shown, one can see that good agreement was obtained for the deflection predictions with the corresponding experimental data.

Appendix A: Strain-Energy Components

For reference, the complete expressions for the strain-energy components U_1 to U_7 are given herein.

$$U_1 = \frac{1}{2}\iint\Bigg[A_{11}\left(\frac{\partial u}{\partial x}\right)^2 + 2A_{12}\left(\frac{\partial u}{\partial x}\right)\left(\frac{\partial v}{\partial y}\right) + A_{22}\left(\frac{\partial v}{\partial y}\right)^2 + 2A_{16}\left(\frac{\partial u}{\partial x}\right)\left(\frac{\partial u}{\partial y}+\frac{\partial v}{\partial x}\right) + 2A_{26}\left(\frac{\partial v}{\partial y}\right)\left(\frac{\partial u}{\partial y}+\frac{\partial v}{\partial x}\right) + A_{66}\left(\frac{\partial u}{\partial y}+\frac{\partial v}{\partial x}\right)^2\Bigg]\,dx\,dy$$

$$U_2 = \frac{1}{2}\iint\Bigg\{A_{11}\left(\frac{\partial u}{\partial x}\right)\left(\frac{\partial w}{\partial x}\right)^2 + A_{12}\left[\left(\frac{\partial u}{\partial x}\right)\left(\frac{\partial w}{\partial y}\right)^2 + \left(\frac{\partial v}{\partial y}\right)\left(\frac{\partial w}{\partial x}\right)^2\right] + A_{16}\left[2\left(\frac{\partial u}{\partial x}\right)\left(\frac{\partial w}{\partial x}\right)\left(\frac{\partial w}{\partial y}\right) + \left(\frac{\partial u}{\partial y}+\frac{\partial v}{\partial x}\right)\left(\frac{\partial w}{\partial x}\right)^2\right] + A_{26}\left[2\left(\frac{\partial v}{\partial y}\right)\left(\frac{\partial w}{\partial x}\right)\left(\frac{\partial w}{\partial y}\right) + \left(\frac{\partial u}{\partial y}+\frac{\partial v}{\partial x}\right)\left(\frac{\partial w}{\partial y}\right)^2\right] + A_{22}\left(\frac{\partial v}{\partial y}\right)\left(\frac{\partial w}{\partial y}\right)^2 + 2A_{66}\left(\frac{\partial u}{\partial y}+\frac{\partial v}{\partial x}\right)\left(\frac{\partial w}{\partial x}\right)\left(\frac{\partial w}{\partial y}\right)\Bigg\}\,dx\,dy$$

$$U_4 = \iint\Bigg[B_{11}\left(\frac{\partial u}{\partial x}\right)\left(\frac{\partial \phi}{\partial x}\right) + B_{12}\left(\frac{\partial u}{\partial x}\right)\left(\frac{\partial \theta}{\partial y}\right) + B_{16}\left(\frac{\partial u}{\partial x}\right)\left(\frac{\partial \theta}{\partial x}+\frac{\partial \phi}{\partial y}\right) + B_{12}\left(\frac{\partial v}{\partial y}\right)\left(\frac{\partial \phi}{\partial x}\right) + B_{22}\left(\frac{\partial v}{\partial y}\right)\left(\frac{\partial \theta}{\partial y}\right) + B_{26}\left(\frac{\partial v}{\partial y}\right)\left(\frac{\partial \theta}{\partial x}+\frac{\partial \phi}{\partial y}\right) + B_{16}\left(\frac{\partial u}{\partial y}+\frac{\partial v}{\partial x}\right)\left(\frac{\partial \phi}{\partial x}\right) + B_{26}\left(\frac{\partial u}{\partial y}+\frac{\partial v}{\partial x}\right)\left(\frac{\partial \theta}{\partial y}\right) + B_{66}\left(\frac{\partial u}{\partial y}+\frac{\partial v}{\partial x}\right)\left(\frac{\partial \theta}{\partial x}+\frac{\partial \phi}{\partial y}\right)\Bigg]\,dx\,dy$$

$$U_5 = \frac{1}{2}\iint\Bigg[B_{11}\left(\frac{\partial w}{\partial x}\right)^2\left(\frac{\partial \phi}{\partial x}\right) + B_{12}\left(\frac{\partial w}{\partial x}\right)^2\left(\frac{\partial \theta}{\partial y}\right) + B_{16}\left(\frac{\partial w}{\partial x}\right)^2\left(\frac{\partial \theta}{\partial x}+\frac{\partial \phi}{\partial y}\right) + B_{12}\left(\frac{\partial w}{\partial y}\right)^2\left(\frac{\partial \phi}{\partial x}\right) + B_{22}\left(\frac{\partial w}{\partial y}\right)^2\left(\frac{\partial \theta}{\partial y}\right) + B_{26}\left(\frac{\partial w}{\partial y}\right)^2\left(\frac{\partial \theta}{\partial x}+\frac{\partial \phi}{\partial y}\right) + 2B_{16}\left(\frac{\partial w}{\partial x}\right)\left(\frac{\partial w}{\partial y}\right)\left(\frac{\partial \phi}{\partial x}\right) + 2B_{26}\left(\frac{\partial w}{\partial x}\right)\left(\frac{\partial w}{\partial y}\right)\left(\frac{\partial \theta}{\partial y}\right) + 2B_{66}\left(\frac{\partial w}{\partial x}\right)\left(\frac{\partial w}{\partial y}\right)\left(\frac{\partial \theta}{\partial x}+\frac{\partial \phi}{\partial y}\right)\Bigg]\,dx\,dy$$

$$U_6 = \frac{1}{2}\iint\Bigg[D_{11}\left(\frac{\partial \phi}{\partial x}\right)^2 + 2D_{12}\left(\frac{\partial \phi}{\partial x}\right)\left(\frac{\partial \theta}{\partial y}\right) + D_{22}\left(\frac{\partial \theta}{\partial y}\right)^2 + 2D_{16}\left(\frac{\partial \phi}{\partial x}\right)\left(\frac{\partial \phi}{\partial y}\right) + 2D_{16}\left(\frac{\partial \phi}{\partial x}\right)\left(\frac{\partial \theta}{\partial x}\right) + 2D_{26}\left(\frac{\partial \theta}{\partial y}\right)\left(\frac{\partial \theta}{\partial x}\right) + 2D_{26}\left(\frac{\partial \phi}{\partial y}\right)\left(\frac{\partial \theta}{\partial y}\right) + D_{66}\left(\frac{\partial \phi}{\partial y}\right)^2 + 2D_{66}\left(\frac{\partial \phi}{\partial y}\right)\left(\frac{\partial \theta}{\partial x}\right) + D_{66}\left(\frac{\partial \theta}{\partial x}\right)^2\Bigg]\,dx\,dy$$

$$U_7 = \frac{1}{2}\iint\Bigg[G_{55}\phi^2 + 2G_{55}\phi\left(\frac{\partial w}{\partial x}\right) + G_{55}\left(\frac{\partial w}{\partial x}\right)^2 + 2G_{45}\phi\theta + 2G_{45}\phi\left(\frac{\partial w}{\partial y}\right) + 2G_{45}\theta\left(\frac{\partial w}{\partial x}\right) + 2G_{45}\left(\frac{\partial w}{\partial x}\right)\left(\frac{\partial w}{\partial y}\right) + G_{44}\theta^2 + 2G_{44}\theta\left(\frac{\partial w}{\partial y}\right) + G_{44}\left(\frac{\partial w}{\partial y}\right)^2\Bigg]\,dx\,dy$$

$$W = \iint pw\,dx\,dy + \int \bar{N}^T \cdot \boldsymbol{u}\,ds$$

with p, distributed transverse pressure, and $\bar{N}^T$ applied forces at the boundary.

Appendix B: Displacement Modes

For a plate simply supported on all sides, one can use series of trigonometric functions

$$w_{ss} = \sum_i \sum_j w_{ij} \sin(i\pi\xi)\sin(j\pi\eta)$$

$$\phi_{ss} = \sum_i \sum_j \phi_{ij}\frac{i\pi}{a}\cos(i\pi\xi)\sin(j\pi\eta)$$

$$\theta_{ss} = \sum_i \sum_j \theta_{ij}\frac{i\pi}{b}\sin(i\pi\xi)\cos(j\pi\eta)$$

For a plate clamped on all sides, a double series of beam functions can be used

$$w_{cc} = \sum_i \sum_j w_{ij}F_i(\xi)F_j(\eta)$$

$$\phi_{cc} = \sum_i \sum_j \phi_{ij}\frac{1}{a}F_i'(\xi)F_j(\eta)$$

$$\theta_{cc} = \sum_j \sum_j \theta_{ij}\frac{1}{b}F_i(\xi)F_j'(\eta)$$

Acknowledgments

This work was sponsored by a joint Navy/Federal Aviation Administration endeavor under Contract N00019-85-C-0090. Part of the analysis work was developed by the first author at the Laboratoire des Techniques Aeronautiques et Spatiales at the University of Liege (Belgium) under the direction of the late Professor Guy Sander, to whom the first author is forever deeply indebted.

References

[1]Leissa, A. W., "Buckling of Laminated Composite Plates and Shell Panels," Air Force Wright Aeronautical Laboratories, Wright-Patterson Air Force Base, OH, AFWAL-TR-85-3069, June 1985.

[2]Reissner, E., "The Effect of Transverse Shear Deformation on the Bending of Elastic Plates," *Journal of Applied Mechanics*, Vol. 12, June 1945, pp. A69–A77.

[3]Mindlin, R. D., "Influence of Rotatory Inertia and Shear on Flexural Motion of Isotropic Elastic Plates," *Journal of Applied Mechanics*, Vol. 18, March 1951, pp. 31–38.

[4]Reddy, J. N., "A Refined Nonlinear Theory of Plates with Transverse Shear Deformation," *International Journal of Solids and Structures*, Vol. 20, Sept.–Oct. 1984, pp. 881–896.

[5]Rao, K. M., "Buckling Analysis of Anisotropic Sandwich Plates Faced with Fiber-Reinforced Plastics," *AIAA Journal*, Vol. 23, Aug. 1985, pp. 1247–1253.

[6]Benson, A. S. and Mayers, J., "General Instability and Face Wrinkling of Sandwich Plates: Unified Theory and Applications," *AIAA Journal*, Vol. 5, April 1967, pp. 729–739.

[7]Arnolds, R. R. and Mayers, J., "Buckling, Postbuckling and Crippling of Materially Nonlinear Laminated Composite Plates,"

International Journal of Solids and Structures, Vol. 20, Sept.–Oct. 1984, pp. 863–880.

[8]Minguet, P. J., "Buckling of Graphite/Epoxy Sandwich Plates," M.S. Thesis, Dept. of Aeronautics and Astronautics, Massachusetts Institute of Technology, Cambridge, MA, May 1986; also, Technology Laboratory for Advanced Composites Rept. 86-16, MIT, May 1986.

[9]Whitney, J., "Stress Analysis of Thick Laminated Composite and Sandwich Plates," *Journal of Composite Materials*, Vol. 6, Oct. 1972, pp. 426–440.

[10]Dugundji, J., "Simple Expressions for Higher Vibration Modes of Uniform Euler Beams," *AIAA Journal*, Vol. 26, Aug. 1988, pp. 1013, 1014.

[11]Minguet, P. J., "Reference Manual for POSTBS, Postbuckling Analysis Program for Laminated Rectangular Plates," Massachusetts Institute of Technology, Cambridge, MA, TELAC Rept. 87-18, Nov. 1987.

[12]Jensen, D. W., "Buckling and Postbuckling Behavior of Unbalanced and Unsymmetric Laminated Graphite/Epoxy Plates," Ph.D. Thesis, Dept. of Aeronautics and Astronautics, Massachusetts Institute of Technology, Cambridge, MA, Jan. 1986, also, TELAC Rept. 86-3, MIT, Jan. 1986.

[13]Dinardo, M. T., "Buckling and Postbuckling Behavior of Laminated Composite Plates with Ply Dropoffs," M.S. Thesis, Dept. of Aeronautics and Astronautics, Massachussets Institute of Technology, Cambridge, MA, May 1986, also, TELAC Rept. 86-13, MIT, May 1986.

[14]Minguet, P. J., Dugundji, J., and Lagace, P. A., "Buckling and Failure of Sandwich Plates with Graphite/Epoxy Faces and Various Cores," *Journal of Aircraft*, Vol. 25, April 1988, pp. 372–379.